Transient modelling of pumped two-phase cooling systems: Comparison between experiment and simulation

Henk Jan van Gerner[1]
National Aerospace Laboratory NLR, Amsterdam, The Netherlands

and

Niels Braaksma[2]
ASML, Veldhoven, The Netherlands

Two-phase pumped cooling systems are applied when it is required to maintain a very stable temperature in a system, for example in the AMS02, which was launched with a space shuttle (in May 2011) and subsequently mounted on the International Space Station. However, a two-phase pumped cooling system can show complex transient behavior in response to heat load variations. For example, when the heat load is increased, a large volume of vapor is suddenly created, which results in a liquid flow into the accumulator and an increase in the pressure drop. This will result in variations in the temperature in the system, which are undesired. It is necessary to calculate these temperature variations before an application is being built. For this reason, a software tool for transient two-phase systems has been developed by NLR. This tool numerically solves the one-dimensional time-dependent compressible Navier-Stokes equations, and includes the thermal masses of all the components. The tool has been used for different projects, and the numerical results show an excellent agreement with experiments. In this paper, several pumped two-phase cooling systems are discussed, and a comparison between simulations and experiments is presented.

Nomenclature

Δt	- Time step (s)
Δx	- Length interval (m)
ρ	- Fluid density (kg/m^3)
$\bar{\bar{\tau}}$	- Viscous stress tensor (N/m^2)
A	- Surface area (m^2)
C	- CFL condition constant (-)-
c_p	- Specific heat (J/(kg K))
d	- Inner diameter tube (m)
E	- Specific total energy of the fluid (J/kg)
g_x	- Gravitational acceleration in the travel direction (m/s^2)
H	- Specific total enthalpy fluid (J/kg)
H_{internal}	- Specific internal enthalpy of the fluid (J/kg)
h	- Heat transfer coefficient (W/(m^{2}K))
h_{lv}	- Specific latent heat of vaporization (J/kg)
i	- Index for element in a component (-)
L	- Length of tube or evaporator (m)
$\dot{m}$	- Mass flow (kg/s)
$m_{\text{component}}$	- Mass of a component (kg)
n	- Index for timestep (-)
NE	- Number of elements in a component (-)

[1] R&D Engineer, Space Systems, Henk.Jan.van.Gerner@nlr.nl, +31 88 511 4628.
[2] R&D Engineer, TE RES Research F&T, Niels.Braaksma@asml.com, +31 6 11 30 9536

P_{in}, P_{out} - Power input in component, Power out of condenser (W)
p, p_{sat} - Pressure, Saturation pressure (N/m^2)
Q - Volumetric heat input (W/m^3)
Re - Reynolds number (-)
T, T_{sat} - Temperature fluid, Saturation temperature (K)
t - Time (s)
u - Fluid velocity (m/s)
X - Vapor mass fraction (-)
x - Distance (m)
V - Volume (m^3)

I. Introduction

Two-phase pumped cooling systems are applied when it is required to maintain a very stable temperature in a system, or when the tubing for a cooling system must have a small diameter. This paper discusses a software tool to calculate the behavior of two-phase pumped cooling systems. The software tool has been used for different systems and customers, e.g. for Thales Alenia Space (for a space application) and ASML (for several terrestrial systems). The experimental work and part of the modelling work in this paper has been carried out by Niels Braaksma at ASML as part of a MSc thesis. ASML is the largest supplier in the world of photolithography systems for the semiconductor industry.

II. Two-phase Mechanically Pumped Fluid Loop

In a Two-phase Mechanically Pumped Fluid Loop (2Φ-MPFL), a pump is used to circulate a working fluid. Downstream of the pump, the fluid first flows to an evaporator, where liquid is evaporated, while heat from the payload is being absorbed. The vapor then flows to a condenser where it is condensed back into liquid. The saturation pressure (and thereby the saturation temperature) in the system is controlled by the accumulator. One of the advantages of a two-phase system is that the temperature of the liquid/vapor mixture is the same in the entire system (assuming that the pressure drop is small), and independent of the heat input. This in contrast to a single-phase (e.g. liquid water) cooling system, where heat input results in a temperature increase of the liquid. Furthermore, the required mass flow for a two-phase pumped system is much smaller than for a single-phase cooling system, because the heat of evaporation h_{lv} of a fluid is much larger than the specific heat capacity of a fluid times the allowed temperature gradient (i.e. $c_p \Delta T$). This results in a much smaller tubing diameter for a two-phase system than for a single-phase pumped loop. Because of these reasons, a two-phase pumped system was selected for the thermal control system of the tracker instrument of the Alpha Magnetic Spectrometer (AMS02, see next chapter). The subcooled liquid from the condenser can have a very low temperature. In most applications, a heat exchanger is applied in which heat from the vapor/liquid is used to warm the cold liquid to near saturation temperature. A schematic drawing of a 2Φ-MPFL with heat exchanger is shown in Figure 1.

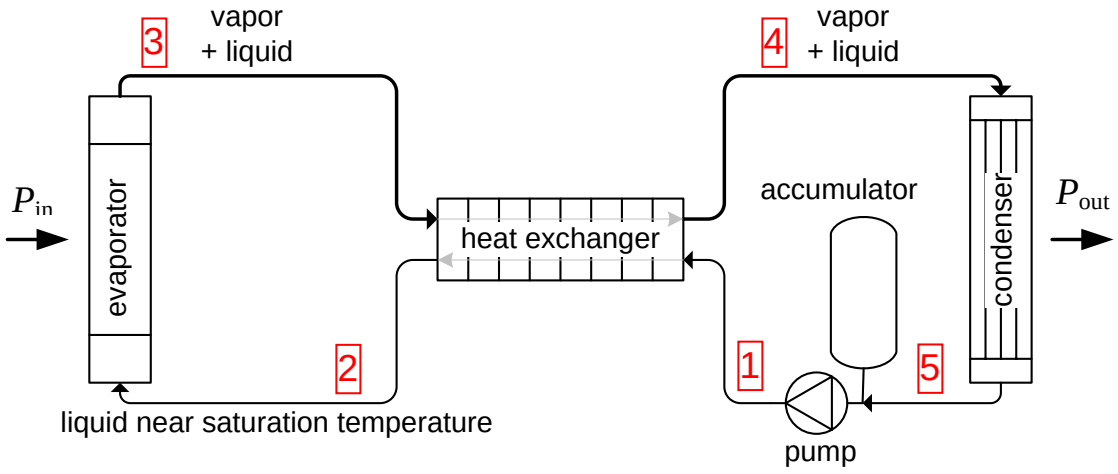

Figure 1 Schematic drawing of a 2Φ-MPFL with heat exchanger. The red numbers 1 to 5 correspond to the numbers in the pressure-enthalpy diagram in Figure 3

III. 2Φ-MPFL for space and terrestrial applications

A two-phase pumped thermal control system has been developed by the NLR for the Alpha Magnetic Spectrometer (AMS02, see Figure 2 for a photo). AMS02 is a large (8500 kg, 2 billion dollar) particle detector that has been launched with the space shuttle in May 2011, after which it was mounted on the International Space Station[1]. Since then, the two-phase thermal control system keeps the AMS02 particle detector at a very stable temperature (fluctuations less than 0.3°C) in a strongly fluctuating thermal environment[2]. The thermal control system uses CO2 as refrigerant because it has the best thermal performance[6].

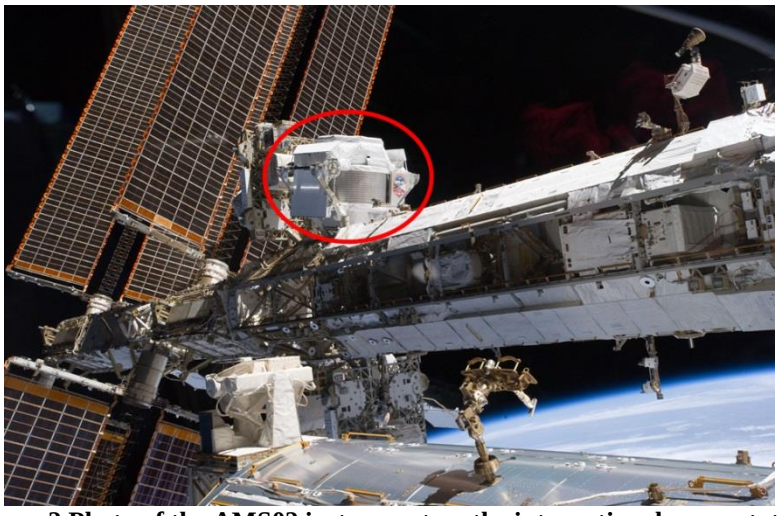

Figure 2 Photo of the AMS02 instrument on the international space station[1]

Two-phase pumped thermal control systems are also being developed for terrestrial applications. For example, in the lithography machines of the company ASML, large heat loads have to be removed with very light-weight and small systems. Several two-phase thermal control prototypes have been built and modelled, some of which achieve a temperature stability of 0.001°C with varying heat load.

IV. Why is a numerical model required?

A 2Φ-MPFL is usually applied when a uniform system temperature is required. This can be achieved easily with a steady-state heat load. However, when the heat load on the evaporator of a 2Φ-MPFL changes, liquid will flow into or out of the accumulator. As a result, the pressure in the accumulator will change, and therefore the system saturation temperature. The accumulator can respond by heating/cooling inside the accumulator in order to return to the desired temperature. In principle, the accumulator can maintain exactly the desired temperature in the system when the accumulator cooling capacity is very large or when the accumulator is very big. In practice however, the cooling capacity and accumulator size are limited and the system temperature will vary. An accurate model of the complete system is required to calculate how much the temperature will vary.

V. Physical-mathematical model

A. Time-dependent 1D Navier-Stokes equation

The fluid flow in a 2Φ-MPFL can be modelled with the one-dimensional time-dependent compressible Navier-Stokes equations:

$$\frac{\partial \rho}{\partial t} + \frac{\partial \rho u}{\partial x} = 0 \quad \rightarrow \text{mass equation} \tag{1}$$

$$\frac{\partial \rho u}{\partial t} + \frac{\partial \rho u^2}{\partial x} = -\frac{\partial p}{\partial x} + \frac{\partial \bar{\bar{\tau}}}{\partial x} + \rho g_x \rightarrow \text{momentum equation} \tag{2}$$

$$\frac{\partial \rho E}{\partial t} + \frac{\partial \rho u E}{\partial x} = Q - \frac{\partial p u}{\partial x} + \frac{\partial u \bar{\bar{\tau}}}{\partial x} + \rho u g_x \rightarrow \text{energy equation} \tag{3}$$

$$\rho(p, E_{\text{internal}}) \rightarrow \text{equation of state (with } E_{\text{internal}} = E - \tfrac{1}{2}u^2 \text{)} \tag{4}$$

In these equations, it is assumed that the liquid and vapor in a mixed flow have the same temperature and velocity (i.e. the homogeneous flow model is assumed).

The energy E and enthalpy H are related via $E=H-p/\rho$. The energy conservation equation can therefore be rewritten into the enthalpy conservation equation:

$$\frac{\partial \rho H}{\partial t} + \frac{\partial \rho u H}{\partial x} = Q + \frac{\partial p}{\partial t} + \frac{\partial u \overline{\overline{\tau}}}{\partial x} + \rho u g_x \rightarrow \text{enthalpy equation} \tag{5}$$

which can be rewritten into:

$$\rho \frac{\partial H}{\partial t} + \left(H \frac{\partial \rho}{\partial t} + H \frac{\partial \rho u}{\partial x} \right) + \rho u \frac{\partial H}{\partial x} = Q + \frac{\partial p}{\partial t} + \frac{\partial u \overline{\overline{\tau}}}{\partial x} + \rho u g_x \tag{6}$$

$\left(H \frac{\partial \rho}{\partial t} + H \frac{\partial \rho u}{\partial x} \right)$ = 0, see Eq.(1)

B. Simplification

Solving the complete Navier-Stokes set of equations can be very time consuming. For this reason, the set of equations is simplified:

- Only the mass equation (1) and enthalpy equation (6) are initially solved. The momentum equation (2) is not solved directly. As a result, pressure waves (travelling with the speed of sound) cannot be simulated with this method. This greatly reduces the computation time for the model, since the maximum timestep is now determined by the fluid velocity, instead of the sound velocity (see section VII.E).
- For two-phase pumped loops, pressure transients and viscosity only have a limited influence on the enthalpy equation (e.g. viscous heating is only a few percent of the heat input). For this reason, pressure transients ($\partial p/\partial t$) and the viscosity stress tensor ($\overline{\overline{\tau}}$) are ignored in the enthalpy equation (6).
- Gravity is ignored. For the system described in this paper, gravity has very little influence on the calculated behavior of the system, since no large height differences are present in the system and the pressure differences caused by gravity are negligible compared to the absolute pressure and other pressure differences (e.g. caused by friction). In other simulated systems (not described in this paper), gravity effects are included.

With these simplifications, the enthalpy and mass equation become:

$$\frac{\partial H}{\partial t} = -u \frac{\partial H}{\partial x} + \frac{Q}{\rho} \rightarrow \text{enthalpy equation} \tag{7}$$

$$\frac{\partial u}{\partial x} = -\frac{u}{\rho}\frac{\partial \rho}{\partial x} - \frac{\partial \rho}{\rho \partial t} \rightarrow \text{mass equation} \tag{8}$$

All fluid properties can be derived when two thermodynamic variables are known:

$$\rho(p, H_{\text{internal}}) \rightarrow \text{equation of state (with } H_{\text{internal}} = H - \tfrac{1}{2}u^2 \text{)} \tag{9}$$

For example, Figure 3 shows the pressure-enthalpy diagram for CO_2. This figure shows how the density (blue lines), temperature (red lines), entropy (green lines), and vapor mass fraction (black lines) of CO_2 are related to the pressure and enthalpy. In the example of a cooling cycle in the figure, the CO_2 is evaporated to a vapor mass fraction of 0.7. A heat exchanger is used to preheat the cold liquid from the pump to near saturation temperature (between 1 and 2) by using energy from the vapor that leaves the evaporator (between 3 and 4). The underlying data for this diagram (which is obtained with Refprop[3]) can be used to calculate the density, temperature, entropy, and vapor mass fraction at a certain pressure and enthalpy.

The pressure drop ($\partial p/\partial x$) in Eq.(2) consists of a viscous term and a term caused by the momentum change of the fluid. The viscous pressure drop is calculated with (empirical) pressure drop correlations:

$$\frac{\partial p_{\text{viscous}}}{\partial x} = f(u, \rho, H, d) \tag{10}$$

With the use of Eq.(1), the pressure drop due to the momentum change can be written as:

$$\frac{\partial p_{\text{momentum}}}{\partial x} = -\rho \frac{\partial u}{\partial t} - \rho u \frac{\partial u}{\partial x} \tag{11}$$

C. Calculation of heat input *Q* and component temperature

The fluid exchanges heat with the component (tube, evaporator, condenser, etc.) through which it flows. The volumetric heat input *Q* to the fluid is calculated with:

$$Q = h(T_{\text{component}} - T)\frac{A_{\text{fluid-componentinterface}}}{V_{\text{fluid in component}}} \tag{12}$$

The temperature of the component is calculated with:

$$\frac{\partial T_{\text{component}}}{\partial t} = \frac{(P - h(T_{\text{component}} - T)A_{\text{fluid-componentinterface}})}{m_{\text{component}} C_{p,\ \text{component}}} \tag{13}$$

The discretization of these equations and the implementation in Matlab is discussed in the next chapter.

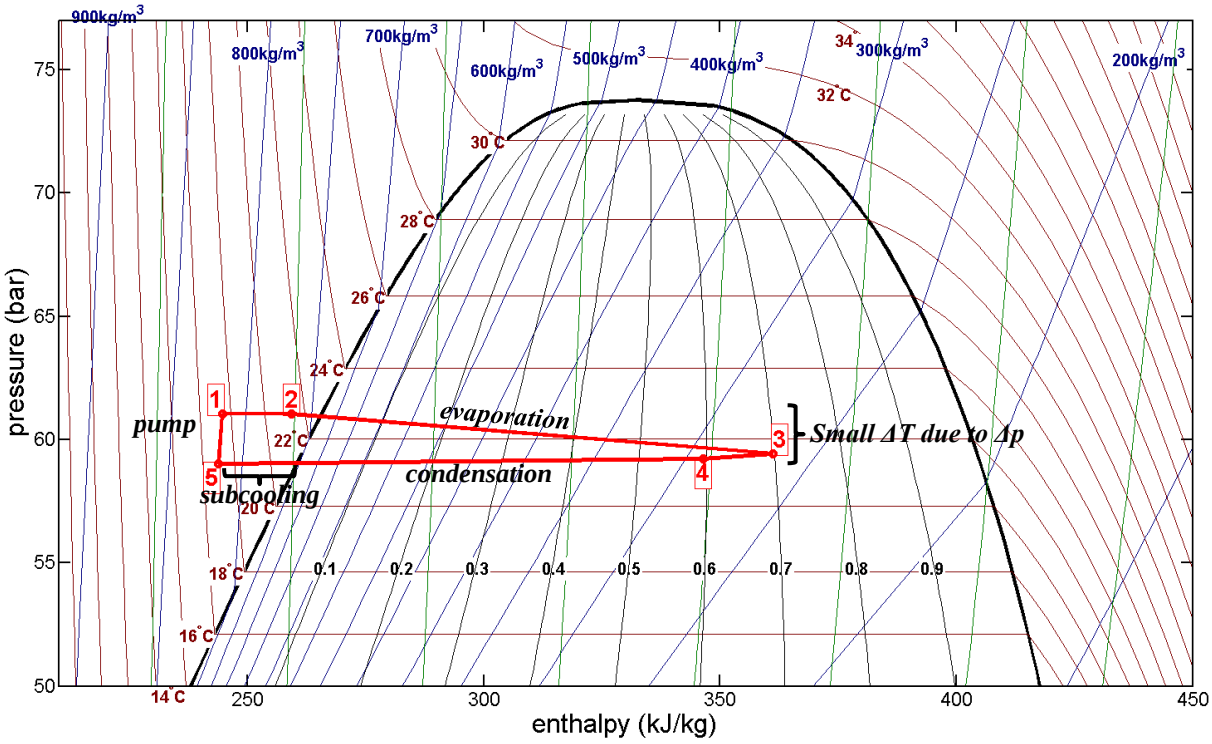

Figure 3 Pressure-Enthalpy diagram of a pumped two-phase cycle with CO_2 (R744). The red numbers 1 to 5 correspond to the locations in figure 1.

VI. Numerical model and implementation

In this chapter, Eq.(7) to Eq.(13) are discretized to make them suitable for numerical implementation.

A. Enthalpy and mass equation

The enthalpy equation (7) is discretized by the MacCormack predictor-corrector scheme. This explicit discretization scheme is very efficient and is one of the simplest stable schemes to implement. Each component (tube, evaporator, condenser etc.) in the 2Φ-MPFL is divided in a number of elements *NE*. First, a predictor value of the enthalpy of elements *i*=1 to *NE* is calculated using the variables at timestep *n* and backward differencing:

$$H_i^p = H_i^n - u_i^n (H_i^n - H_{i-1}^n)\frac{\Delta t}{\Delta x} + \frac{Q_i^n}{\rho_i^n}\Delta t \rightarrow \text{predictor step} \tag{14}$$

after which a predictor density is calculated:

$$\rho_i^p = f(H_i^p, p_i^n) \tag{15}$$

A corrector value of the enthalpy is calculated using predictor values and forward differencing:

$$H_i^c = H_i^n - u_i^n (H_{i+1}^p - H_i^p)\frac{\Delta t}{\Delta x} + \frac{Q_i^n}{\rho_i^p}\Delta t \rightarrow \text{corrector step} \tag{16}$$

The enthalpy at timestep n+1 is the average between the predictor and corrector value:

$$H_i^{n+1} = (H_i^p + H_i^c)/2 \rightarrow \text{averaging step} \tag{17}$$

After which the density at timestep n+1 is calculated:

$$\rho_i^{n+1} = f(H_i^{n+1}, p_i^n) \tag{18}$$

The velocity is calculated by discretizing the mass equation (8) using forward differencing:

$$u_{i+1}^{n+1} = u_i^{n+1} - \frac{u_i^{n+1}}{\rho_i^{n+1}}(\rho_{i+1}^{n+1} - \rho_i^{n+1}) - \frac{(\rho_i^{n+1} - \rho_i^n)}{\rho_i^n}\frac{\Delta x}{\Delta t} \tag{19}$$

B. Pressure drop equation

The frictional pressure drop is calculated using the empirical Muller-Steinhagen & Heck pressure drop correlation in which the friction factor is calculated with the Colebrook equation when the flow is turbulent (Re>4000), and with 64/Re when the flow is laminar (Re<2400). In the intermediary region (2400<Re<4000), a smoothing function between the turbulent and laminar friction factor is used.

$$\frac{\Delta p_{\text{viscous}}}{\Delta x} = f(u_i^{n+1}, \rho_i^{n+1}, H_i^{n+1}, d) \rightarrow \text{empirical pressure drop relation} \tag{20}$$

The momentum pressure drop equation (11) is discretized as:

$$\frac{\Delta p_{\text{momentum}}}{\Delta x} = -\rho_i^{n+1}\frac{(u_i^{n+1} - u_i^n)}{\Delta t} - \rho_i^{n+1}u_i^{n+1}\frac{(u_{i+1}^{n+1} - u_i^{n+1})}{\Delta x} \tag{21}$$

The 'new' pressure is found by adding the viscous and momentum pressure drop:

$$p_{i+1}^{new} = p_i^{new} + \Delta p_{\text{momentum}} + \Delta p_{\text{viscous}} \tag{22}$$

C. Discretization of heat input *Q* and component temperature

The fluid exchanges heat with the component (tube, evaporator, condenser, etc.) through which it flows. The volumetric heat input Q to the fluid is calculated with:

$$Q_i^n = h(T_{\text{i, component}}^n - T_i^n)\frac{A_{\text{i, fluid-componentinterface}}}{V_{\text{i, fluid in component}}} \tag{23}$$

The temperature of the component is calculated with:

$$T_{\text{i, component}}^{n+1} = T_{\text{i, component}}^n + \frac{(P_i^n - h(T_{\text{i, component}}^n - T_i^n)A_{\text{i, fluid-componentinterface}})}{m_{\text{component}}C_{p\ \text{component}}}\Delta t \tag{24}$$

For the simulations discussed in this paper, the heat transfer coefficient h is calculated with Cooper's pool boiling correlation with dryout model for evaporation[4], and the Shah correlation for condensation[5]. Other heat transfer correlations are also implemented.

D. Equation of state

When the enthalpy and pressure in the fluid have been calculated, the other fluid parameters, like density, temperature and vapor mass fraction can be derived via the equation of state. The program Refprop[3] contains the equations of state for a large number of fluids, and this program can interface with Matlab. However, calling Refprop for each component, at each time step, is computationally very expensive. In order to avoid excessive overhead, fluid tables (which can be imported at the start of a simulation) are created using Refprop This fluid table consists of matrices in which the density ρ, vapor mass fraction X, and temperature T is stored for different values of

p and *H*. During the simulation, the density, vapor mass fraction, and temperature of all elements can be obtained very fast by linear interpolation from this table.

E. Maximum time step for numerical stability

The Courant–Friedrichs–Lewy (CFL) condition is a necessary (but not always sufficient) condition for convergence when solving hyperbolic partial differential equations with an explicit numerical scheme. The reasoning behind this condition is that perturbations must not travel further than one length interval Δx during one time step Δt. For the compressible Navier-Stokes momentum equation, perturbations travel with the sound velocity and a necessary condition for convergence of an explicit scheme is:

$$u_{\text{sound}} \frac{\Delta t}{\Delta x} < 1 \rightarrow \text{CFL stability criterion for compressible Navier-Stokes} \tag{25}$$

However, in the simplified scheme that is used for the dynamic model, perturbations do not travel with the sound velocity, but with the fluid velocity [see the enthalpy equation Eq.(7)]:

$$u_{\text{fluid}} \frac{\Delta t}{\Delta x} < 1 \rightarrow \text{CFL stability criterion for simplified scheme} \tag{26}$$

In a 2Φ-MPFL, the fluid velocity is typically ~1 m/s, while the sound velocity in CO_2 at 22°C is ~450 m/s. This means that when the compressible Navier-Stokes equations are solved, the timestep Δt has to be ~450 times smaller than the timestep with the simplified scheme. This implies that it would take ~450 times longer to solve the compressible Navier-Stokes equations. In the implemented model, the time step Δt is determined automatically with the CFL condition:

$$\Delta t_{\text{component}} = C \frac{\Delta x_{\text{component}}}{\max(u_{\text{fluid,component}})}, \; \Delta t = \min(\Delta t_{\text{components}}) \tag{27}$$

Where the CFL condition constant *C* is usually 0.9 in the simulations.

F. Accumulator models

The pressure in a 2Φ-MPFL is controlled by the accumulator. For a two-phase fluid, the pressure is related to the temperature and the accumulator therefore controls the saturation temperature in the system. Two types of accumulators are possible; Pressure Controlled Accumulators (PCA) and Heat Controlled Accumulators (HCA). In a PCA, only subcooled liquid and no vapor is present in the accumulator. The pressure of the liquid in the accumulator can be controlled mechanically, for example by a bellows that is pressurized with an actuator or by pressurized air. The main advantage of a PCA is that it responds very fast. The main disadvantage is that it is relative complex. The pressure/temperature in the HCA can be increased by creating vapor or decreased by creating liquid (i.e. by condensing vapor). This can be achieved for example by a heater that is always submerged in liquid, and a cooling mantle at the top of the accumulator (see Figure 4 for a schematic drawing of the HCA). The main advantage of a HCA is that it is relative simple. The main disadvantage is that the cooling capacity is usually limited, which results in a slow response to changes in evaporator heat input. Besides the heat inputs that are applied to the HCA (i.e. $P_{\text{heat in HCA}}$ and $P_{\text{cool in HCA}}$), there is also internal heat exchange between the vapor and liquid ($P_{\text{vapor to liquid}}$) and between the wall and the fluid ($P_{\text{wall to fluid}}$) when the HCA is not in thermal equilibrium. Both PCA and HCA are modelled and have been used in simulations. The simulations and experiments described in this report have been carried out with a HCA. Note that for terrestrial applications, accumulator design is relative straightforward, since the liquid and vapour are separated by gravity. For space applications, capillary forces are used to ensure that liquid is always present at the inlet/outlet tube of the accumulator. For example for AMS02, a stainless steel mesh screen that is folded into a fan like structure (where the gap between mesh layers becomes narrower towards the liquid entrance pipe of the accumulator) has been used inside the accumulator[2].

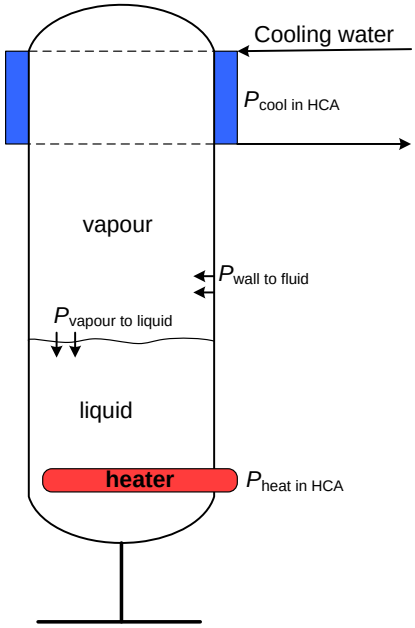

Figure 4 Schematic drawing of the Heat Controlled Accumulator

VII. Comparison with experiments

A. Model description

Figure 5 shows a schematic drawing of the test setup. The preheater (1) is not used during the experiments; it is just a thermal mass. In the evaporator (2), a heat load is applied. In the experiments and simulations, the heat load is varied between 131W and 331W. In actual applications, the object that has to be cooled is often located at a considerable distance from the thermal control system, and for this reason, a 5 m long transport tube is used between the evaporator and the condenser in both the experiments and simulations. The yellow meandering tube in Figure 5 represents this transport tube. The condenser (3) consists of a tube-in-tube heat exchanger that is cooled with liquid water. The water flow is also included in the numerical model. The accumulator (4) is a HCA, with a cooling mantle at the top that provides a cooling power of approximately 47W in the HCA. At the bottom of the HCA, a heater is used to provide heater power. The thermal capacity of the accumulator vessel has a significant effect on the system behavior, and is included in the simulation. The fluid is circulated in the system by the pump (5). Two massflow meters are included in the setup (6). The liquid massflow into the accumulator is equal to the difference in the massflow between the two flow meters. The massflow in the system is controlled to be 3 gr/s. The heating power for the accumulator is controlled with a PID regulator.

Figure 6 shows the calculated steady-state temperature, vapor mass fraction and mass flow in the test-setup with a heat input in the evaporator of 131W. The saturation temperature is controlled by the accumulator to be 22°C. The vapor mass fraction resulting from the heat input is 0.1. Figure 7 shows the calculated temperature, vapor mass fraction and mass flow in the test setup, 6 seconds after the heat input is increased from 131 to 331 W. In the evaporator, the vapor mass fraction is increased to 0.6 due to the increased heat input. This increased vapor mass fraction travels through the system with increased fluid velocity (same mass flow rate, lower fluid density) and is half-way in the transport tube at this time instant. Downstream of this increased vapor front, the massflow is nearly two times higher than upstream of the front, as the fluid adopts the velocity of the front while having a higher density. This excess massflow goes into the accumulator, which results in a higher pressure in the accumulator and therefore a higher saturation temperature in the system. Figure 8 shows the calculated steady-state temperature, vapor mass fraction and mass flow in the test-setup with a heat input in the evaporator of 331W.

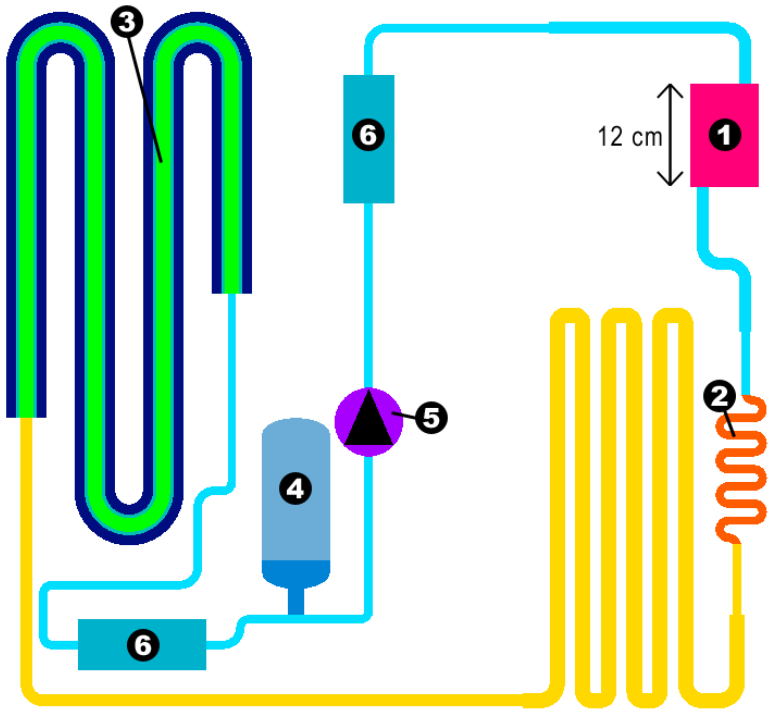

1. Preheater
2. Evaporator
3. Condenser
4. Accumulator
5. Pump
6. Mass flow meters

Figure 5 Schematic drawing of the test setup

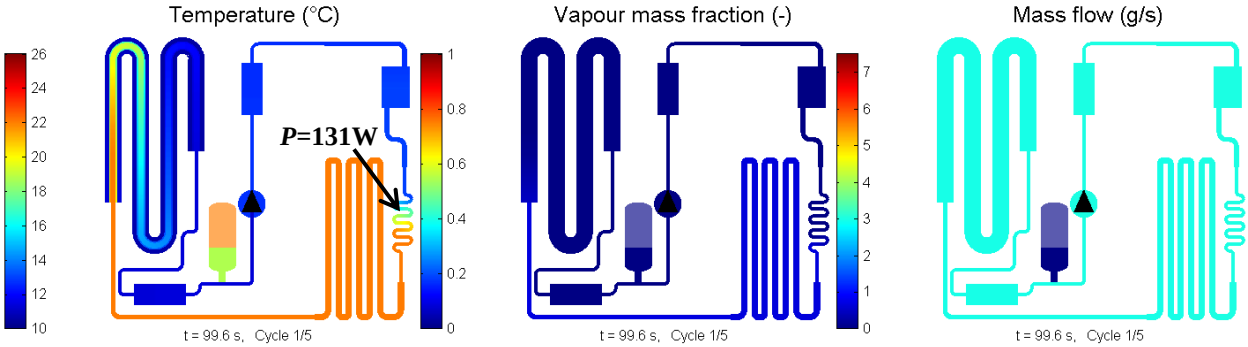

Figure 6 Steady-state temperature, vapor mass fraction, and mass flow for *P*=131 W

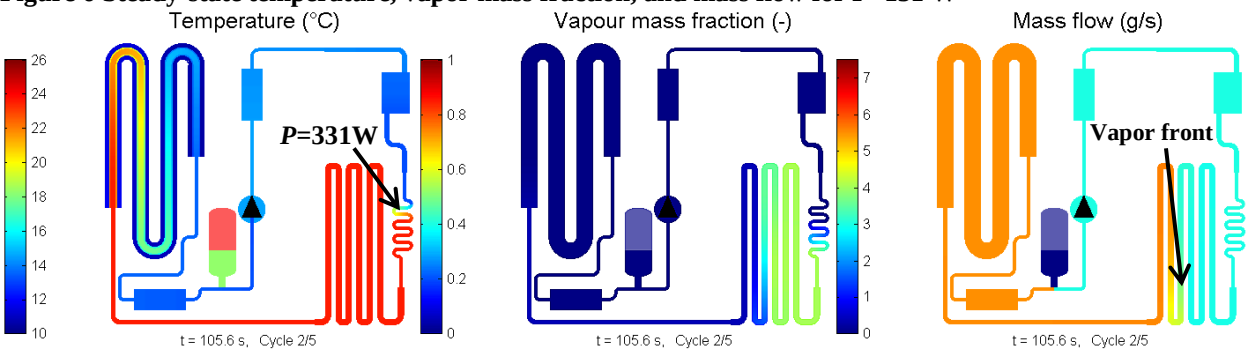

Figure 7 Temperature, vapor mass fraction, and mass flow, 6 seconds after the heat input is changed from 131 to 331 W

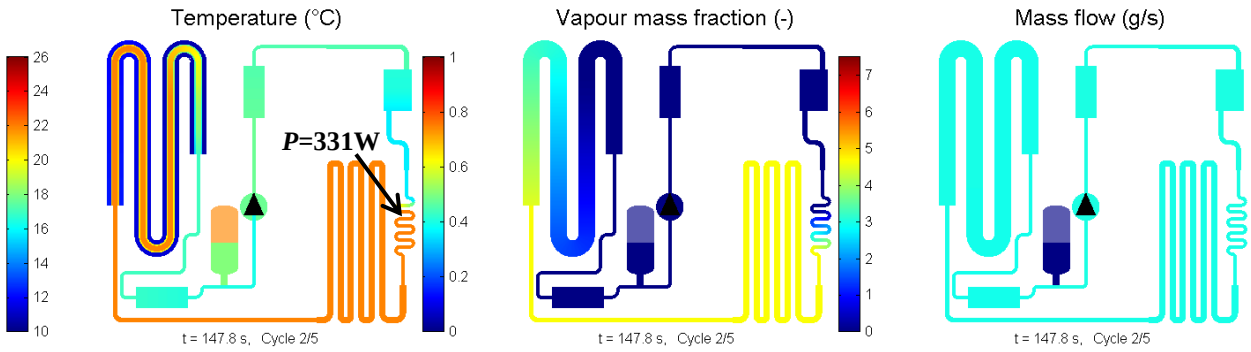

Figure 8 Steady-state temperature, vapor mass fraction, and mass flow for *P*=331 W

B. Experimental setup

Figure 9 shows a photo of the experimental setup and Figure 10 shows a photo of the HCA. The setup has the same components and approximately the same layout as in Figure 5. Figure 11 shows a photo of the 5 m long transport tube.

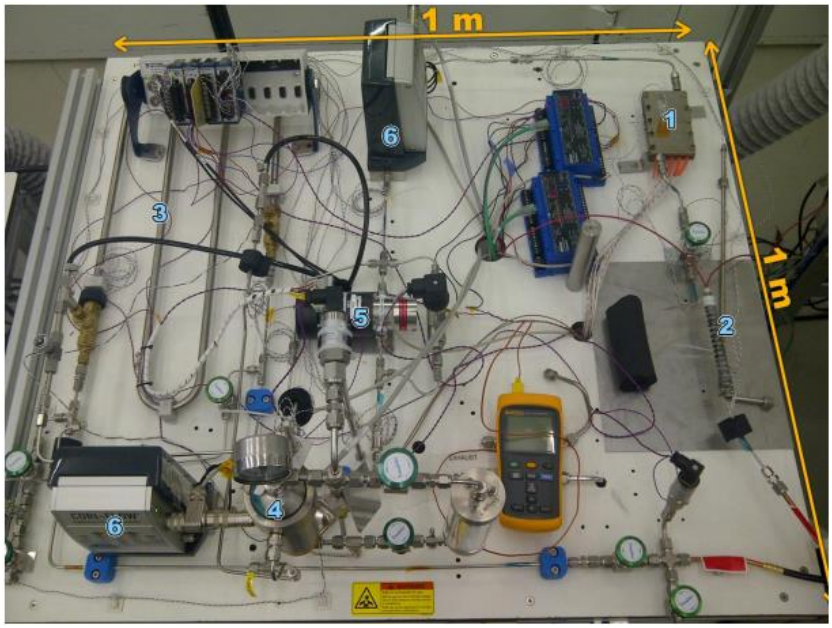

Figure 9 Photo of the experimental setup

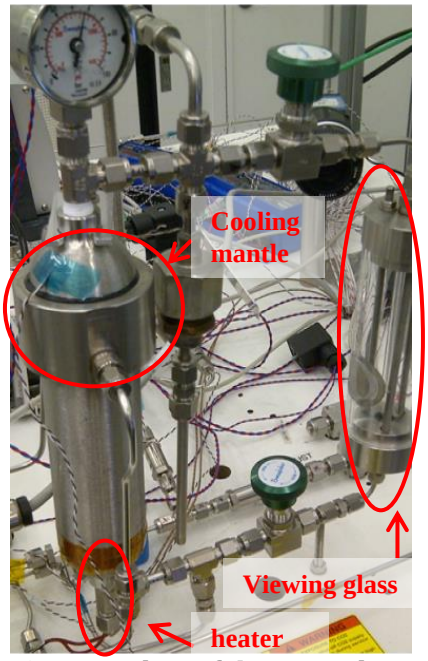

Figure 10 Photo of the accumulator

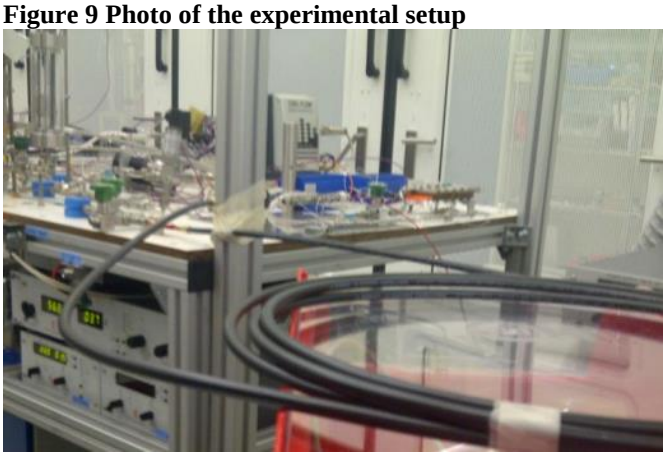

Figure 11 Photo of the 5 m long transport tube

C. Comparison between simulation and experiment

Figure 12 shows the evaporator heat input for both the experiments and simulations. In the left figure, the heat input is increased from 131 to 331W, and in the right figure, the heat input is decreased from 331 to 131W. As a result of an increase in the evaporator heat input, liquid will flow into the accumulator (see Figure 13). The simulated peak is a bit higher and thinner than the experimental peak. An explanation for this is that in the experiment, the evaporator consists of a tube that is soldered to a heater. In the model, it is for simplicity assumed that the wall of the evaporator tube has the same temperature as the heater. In the experiment however, there is a thermal resistance between the tube and the heater, and as a result, the fluid in the evaporator will heat up slightly slower in the experiment than in the simulation. This slightly slower response of the experimental evaporator results in a lower and wider massflow peak into the accumulator. However, the total amount of liquid that flows into the accumulator is the same.

Figure 14 shows the saturation temperature downstream of the evaporator. The PID controller for the accumulator heater tries to keep this saturation temperature at 22°C. However, as a result of the liquid inflow into the accumulator, the saturation temperature in the system will increase. The correspondence between the experiment and simulation is very good, and from this figure it can be concluded that the main objective of the model (i.e. to calculate the variations in the system saturation temperature as a result of changes in the heat load) is achieved. Figure 15 shows the power of the heater in the accumulator. This heater is PID controlled; when the saturation temperature in the system is lower than 22°C, the power will be increased, and when the saturation temperature is higher than 22°C, the power will be decreased. In steady-state, the heater power is equal to the cooling power of the cooling mantle of the accumulator. When fluid flows into the accumulator, the accumulator heater power is quickly reduced to zero, making the accumulator remove heat from the system. The figure shows that initially after an evaporator power change, the simulated and experimental accumulator heater power is very similar. However, the experimental heat power shows much more 'overshoot' than the simulation. The reason for this is not understood, since the PID parameters are the same for both the experiment and simulation. A possible reason could be that the PID controller in the experiment responds differently when the limits of the heater power are reached (i.e. $P_{\text{heat accu}} = 0$ or $P_{\text{heat accu}} = 100$W). Figure 16 shows the temperature upstream of the evaporator. There is a large difference between the simulated and experimental inlet temperature. This difference is caused (among others) by the inaccuracy of the empirical correlation (Shah correlation[5]) that is used to calculate the heat transfer coefficient in the condenser. However, the difference does not influence the system behavior. The reason for this is that a large difference in the liquid temperature before the evaporator, only results in a relative small difference in the vapor mass fraction after the evaporator:

$$\Delta X = \frac{c_p \Delta T}{H_{lv}} \approx 0.1 \text{ for } \Delta T = 4°\text{C} \tag{28}$$

The liquid temperature difference could be reduced by adjusting some parameters (i.e. 'tuning'), but this is not necessary, because the saturation temperature is accurately predicted without any 'tuning' of the results.

In actual thermal control systems, a heat exchanger is usually used to warm the liquid before the evaporator to near saturation temperature (see Figure 1), and in that case, the difference between the simulated and experimental evaporator liquid inlet temperature would become much smaller.

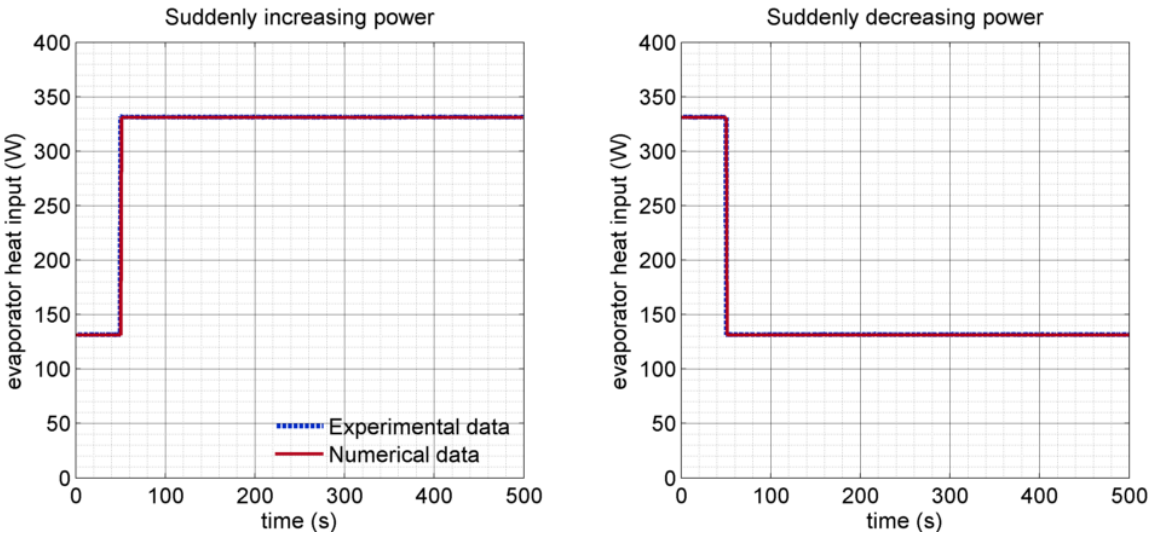

Figure 12 Evaporator heat input for both the experiment and simulation

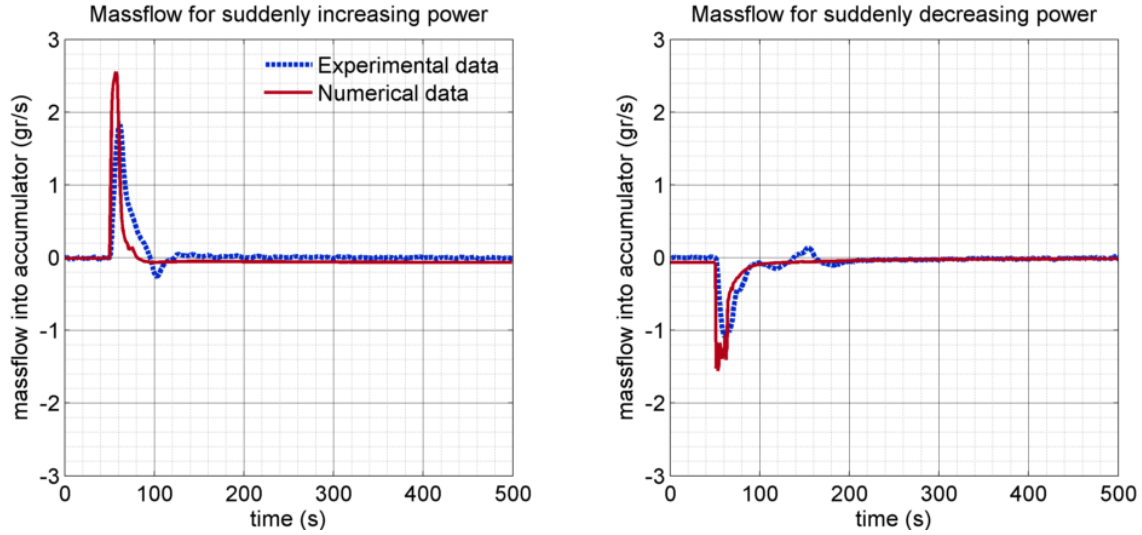

Figure 13 Massflow into the accumulator as a result of an increase and decrease of the heat input

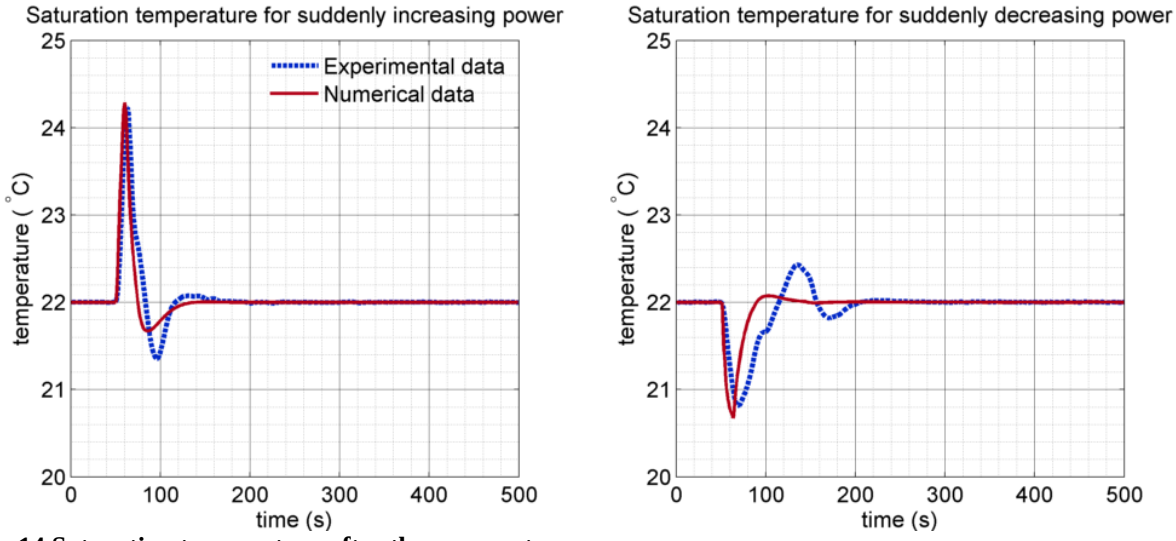

Figure 14 Saturation temperature after the evaporator

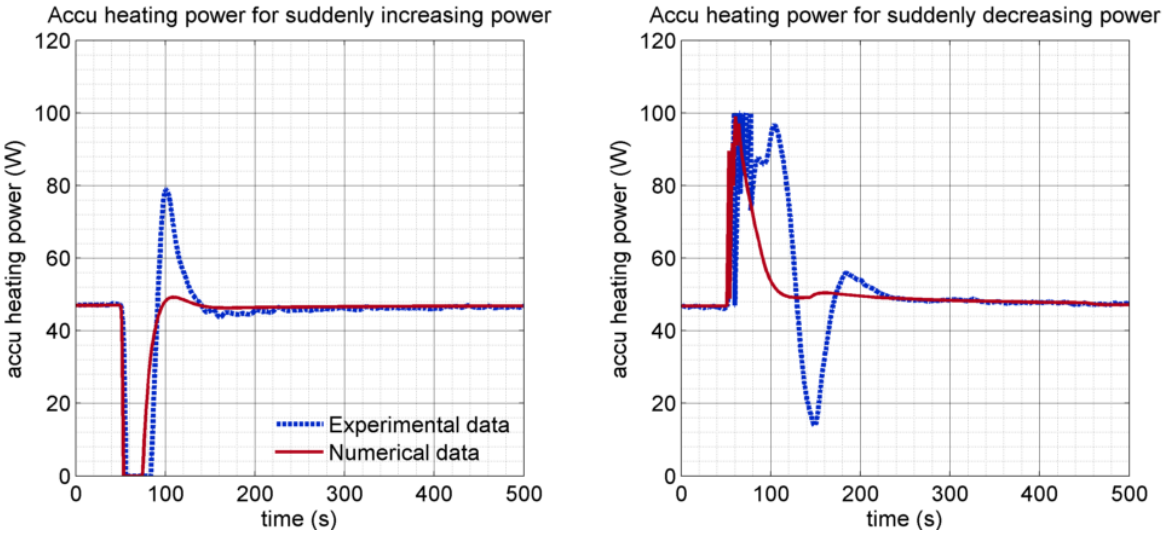

Figure 15 Heating power in the accumulator. This heating power is regulated with a PID controller

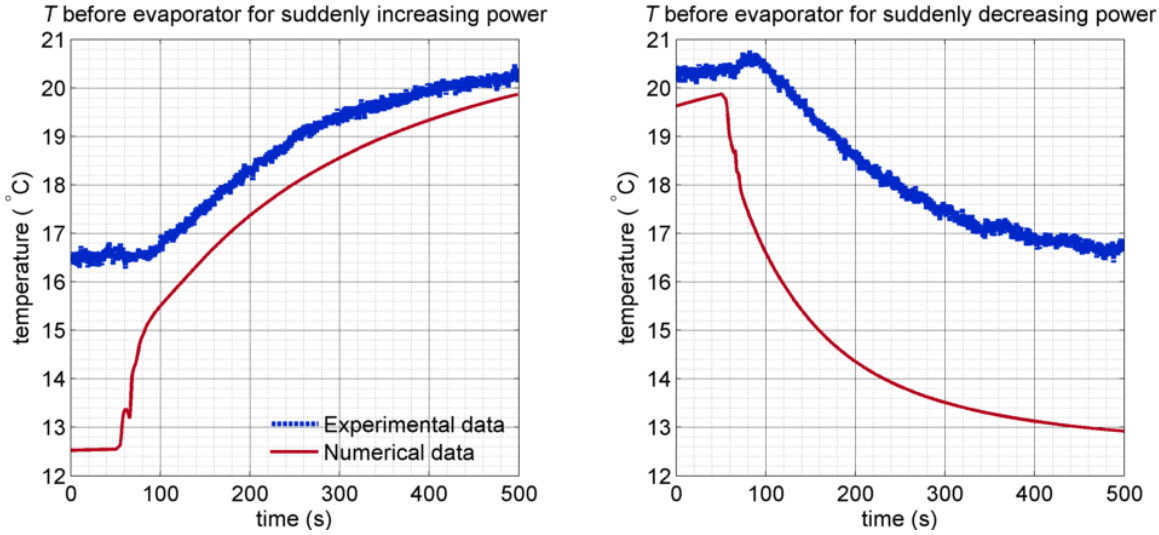

Figure 16 Liquid temperature before the evaporator

VIII. Methods to reduce the temperature variations in a two-phase system

One of the main reasons to use a two-phase thermal control system is that it can maintain a much more stable temperature than a single-phase thermal control system. However, as Figure 14 in the previous chapter shows, the temperature in a two-phase thermal control system can vary significantly when the heat load to the evaporator is suddenly changed. In this chapter, some simple measures that can be used to reduce the temperature variations are discussed. More complex methods are also possible, but are not discussed in this paper.

A. Reduce the diameter (or length) of the transport tube

In the simulations and experiments described in the previous chapter, the internal diameter of the transport tube is 4 mm. When this diameter is smaller, the volume of the transport tube becomes smaller, and this will reduce the amount of liquid that flows into the accumulator when the heat load is increased. As a result, the increase in saturation temperature when the heat load is increased will become smaller, as can be seen in Figure 17. However, the transport tube diameter cannot be made too small. When the diameter is just 1.5 mm, the variations in the pressure drop over the transport tube become too large: The pressure drop over the transport tube increases from 1.8 bar to 3.5 bar when the heat input in the evaporator is increased from 131 to 331W. As a result of this rise in the

pressure drop, the saturation temperature in the evaporator increases. For this reason, the increase in evaporator saturation temperature is larger for a 1.5 mm diameter tube than for a 2 mm diameter tube.

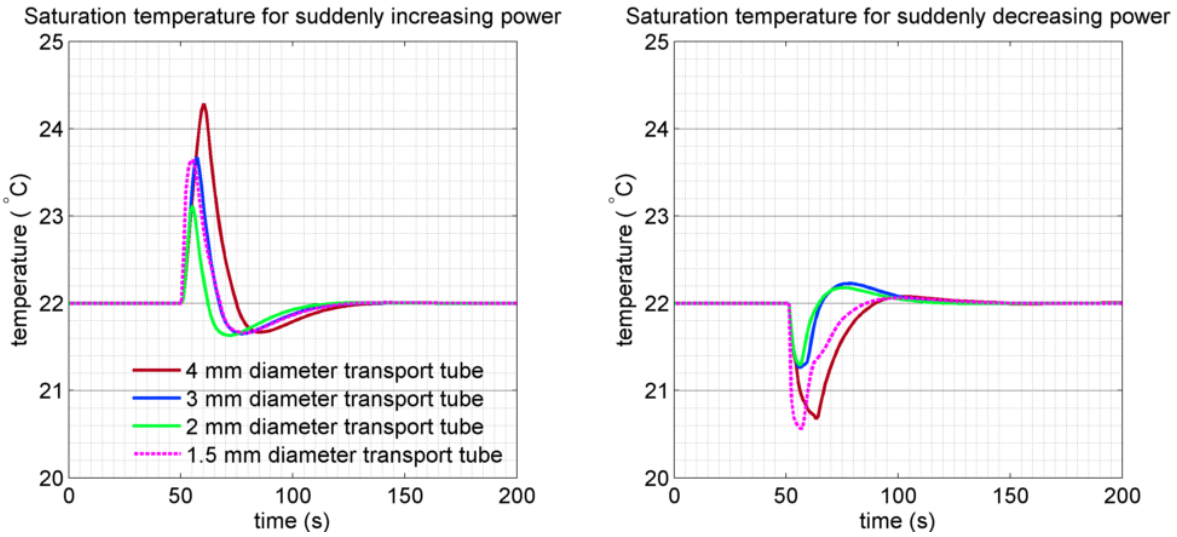

Figure 17 Saturation temperature in the evaporator for different transport tube diameters

B. Increase cooling power in the accumulator

Figure 18 shows the calculated temperature for a simulation in which the cooling power in the accumulator is increased from 47 to 94W. The heating power in the accumulator is also increased with a factor of two. The figure shows that the increase in the accumulator cooling power reduces the variations in the saturation temperature.

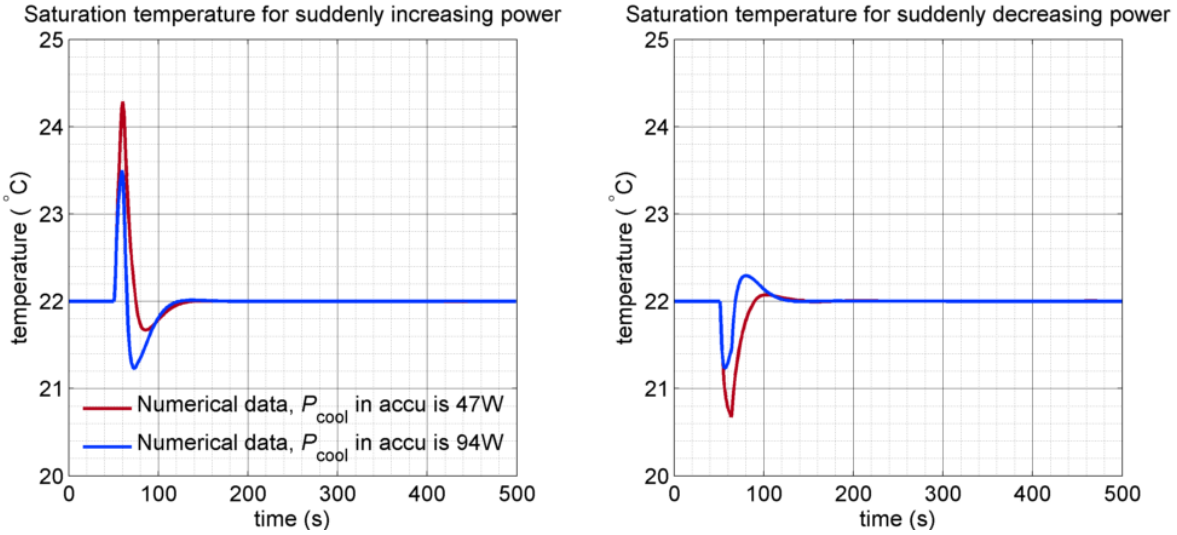

Figure 18 Calculated saturation temperature with 47W and 94W of cooling power in the accumulator

C. Increase the size of the accumulator

When the heat input to the evaporator is increased from 131 to 331W, liquid CO_2 flows into the accumulator. This inflow of liquid compresses the vapor in the accumulator, and as a result, the pressure and saturation temperature in the system rises. In the experiment described in the previous chapter, the volume of the accumulator is 300 ml. When the accumulator volume is 900 ml, the increase in saturation temperature due to an increase in the evaporator heat input is smaller, see Figure 19.

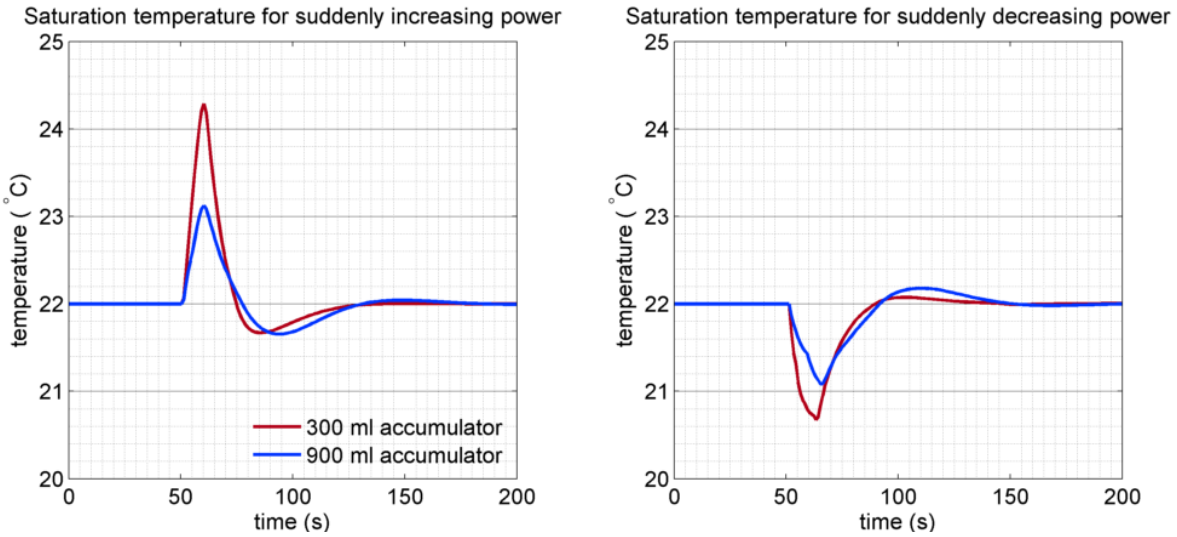

Figure 19 Saturation temperature with two different accumulator volumes

IX. Conclusion

When the heat load on a 2Φ-MPFL changes, liquid will flow into or out of the accumulator. As a result, the pressure in the accumulator will change, and therefore the system saturation temperature. An accurate model of the complete system is required to calculate how much the temperature will vary. For this reason, a software tool that numerically solves the time-dependent mass and enthalpy equation for a two-phase fluid has been developed. The model also includes the thermal capacity of all the solid components. Numerical results have been compared with experiments for different systems (e.g. with a system that keeps a payload at 0.001°C temperature stability), and the correspondence is very good. For other projects, simulations have been carried out with other fluids than CO_2 (e.g. with R134a, R152a and R245fa). However, tests have only been carried out with CO_2. Tests with R134a are planned in order to investigate whether the assumptions that are made in the model (e.g. a homogeneous flow is assumed) are also valid with other fluids.

References

[1]AMS-02, The Alpha Magnetic Spectrometer experiment, URL: http://www.ams02.org/ [cited 20 January 2014]

[2]van Es, J., Pauw A., van Donk G., Laudi E., Gargiulo C., He Z., Verlaat B., Ragnit U., van Leeuwen P., "AMS02 Tracker Thermal Control Cooling System: Test Results of the AMS02 Thermal Vacuum Test in the LSS at ESA ESTEC", AIAA 2012-3577 (2012)

[3]Lemmon, E.W., Huber, M.L., McLinden, M.O. "NIST Standard Reference Database 23: Reference Fluid Thermodynamic and Transport Properties-REFPROP", Version 9.1, National Institute of Standards and Technology, Standard Reference Data Program, Gaithersburg, 2013

[4]Zeynep Ozdemir, M, "Experimental Investigation of CO2, Two-Phase Heat Transfer Characteristics And Prediction Of CO2 Dryout Vapor Quality", MSc thesis, Technical University of Eindhoven, WET 2012.08, 2012.

[5]Shah, M.M., "An Improved And Extended general Correlation for Heat Transfer During Condensation in Plain Tubes", HVAC&R Research, vol. 15, no. 5, pp. 889-913, 2009.

[6]van Gerner, H. J., van Benthem, R. C., van Es, J., Schwaller, D., Lapensée, S., "Fluid selection for space thermal control systems", 44th International Conference on Environmental Systems, ICES-2014-136